A Feasibility Study of Land CSEM Reservoir Monitoring: The Effect of the Airwave

Marwan Wirianto[1], **Wim A. Mulder**[2], **and Evert C. Slob**[1]

[1]Delft University of Technology, Delft, The Netherlands
[2]Shell International Exploration and Production B.V., Rijswijk, The Netherlands

Abstract— The displacement of oil with saline water creates a resistivity change that might be detectable by time-lapse CSEM measurements. Because the difference in measured EM signals before and after production is small, acquisition design plays an important role. We carried out numerical experiments to understand how to optimize the acquisition to best capture the time-lapse signal. Our study shows that exciting a VED source at some distance away from the target would be an attractive choice, as a HED source induces strong airwave energy masking the anomalous signal.

1. INTRODUCTION

Over the last decade, the controlled-source electromagnetic (CSEM) method has established its position as a tool for detecting and evaluating hydrocarbon reservoirs [1]. The method is mainly applied for derisking potential prospects, complementary to seismics. Another potential application is hydrocarbon reservoir monitoring during production. Water flooding or steam injection for oil production creates a resistivity change that may be detectable by time-lapse EM measurements. The main question is whether or not such a change is detectable and if EM can do better than time-lapse seismics. The latter requires a porosity greater than 30% to have a significant velocity difference between a water- and hydrocarbon-bearing reservoir. With EM, the resistivity difference between rock containing hydrocarbons or saline water can be two or three orders of magnitude, making CSEM method potentially more suitable if this difference can be detected in the presence of repeatability errors and noise.

Several authors have investigated the feasibility of CSEM monitoring [2–5]. The first and second groups employed a 3D integral-equation method to model the time-lapse effect due to the flooding front during water injection into an oil reservoir, whereas [4] used an accurate 2D finite-element modeling code to study several scenarios for reservoir depletion, including lateral and bottom flooding, stacked reservoirs, and partial depletion. [5] used a 3D multigrid modeling code of [6] to study the effect of vertically piston-like reservoir depletion in a land setting. To indicate the time-lapse resistivity changes, the authors frequently used both the time-lapse difference as well as the ratio of the recorded EM data before and after production, when part of the oil has been replaced by saline water. In some cases, the data comparison provided direct geometrical information about the depleted zone, whereas in others, more advanced data processing was required. However, the comparison of data recorded at the receivers offers little insight in how the EM fields interact with the depleted zone before and after production. Consequently, a direct interpretation remains difficult even if the time-lapse signals show up clearly.

Here, we present a modeling exercise investigating the interaction between excited low-frequency EM signals and the depleted zone in more detail. We use 2D vector plots of the current density generated by a harmonic electric dipole source in a simple half-space background. The patterns of current distributions are analyzed for two models that represent the resistivity before and after oil production with a water drive. We consider two sources: a surface horizontal electric dipole (HED) source and a vertical electric dipole (VED) source in a well. Understanding how the EM fields interact with the depleted zone can help us to optimize acquisition design.

We first review the basic concept of the CSEM method in the context of the monitoring problem, then present the numerical experiments, and finally discuss our findings.

2. PRIMARY-SECONDARY FORMULATION

To illustrate the concept of the CSEM method for reservoir monitoring, we begin with a simple survey layout. A typical field deployment with a horizontal electric dipole (HED) is sketched in Figure 1. During a survey, a source is employed to excite electromagnetic fields that penetrate through

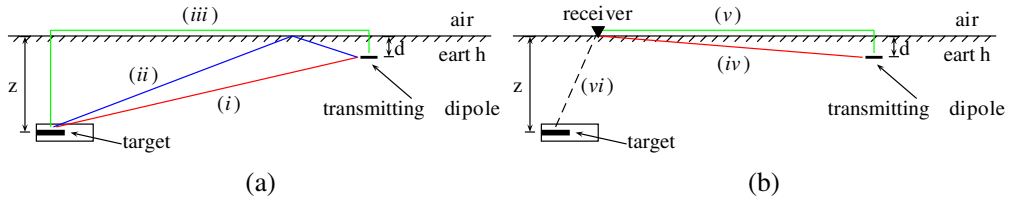

Figure 1: (a) Paths of the EM fields at the depleted zone (target) from a HED source, consisting of the direct field (i), the reflected field (ii), and the airwave (iii). (b) Paths of EM fields at receivers, consisting of the direct field (iv), the direct airwave (v) and the time-lapse field (vi).

the background medium and illuminate the target, in our case the depleted zone (Figure 1(a)). EM receivers are placed on the surface, typically measuring the horizontal electric currents and the three components of the magnetic field. The interaction between the excited low-frequency EM signals and the conductive target zone then results in a secondary field that can be detected with receivers on the surface in addition to the response of the background field (Figure 1(b)). The response of the background field is the EM response that would be excited by the same source in the absence of the target body. The presence of a target body is usually analyzed by comparing the EM response of the target to the response for the background without the target.

The concept of the CSEM method for the monitoring problem is the same as for the exploration problem, but with a different target body and background fields. For exploration, the target body is the resistive hydrocarbon-bearing reservoir and the background field is the response for a background medium without the reservoir. For monitoring, the target body is the depleted zone and the background field is the response for the initial configuration, before oil production started. Although the concepts are similar, the analysis for the monitoring problem differs from that for the exploration case. For exploration, the analysis is frequently done by comparing the EM response of a hydrocarbon-bearing reservoir to the response for a horizontally layered background without the reservoir. The layered background model is used for computational speed and lateral variations are usually accommodated for by locally gluing 1D models together. Because the hydrocarbon reservoir is more resistive than the surrounding background, its presence causes the electromagnetic field to be reflected. It then diffuses back to the receivers at the sea bottom or, in our case, on the land surface, where it can be detected as an anomalous signal. In contrast to data analysis for the exploration problem, the analysis for the monitoring problem usually involves the EM responses for two different states with oil present in both. After production, there still may be oil on top of the water-flooded area. The existence of this highly resistive body may prevent the depleted zone from being "illuminated" by the source and therefore the time-lapse difference in the EM signal may be too weak to be reliably measured. In that case, acquisition design will play an important role in capturing the time-lapse variations. In the next section, we consider some numerical experiments to investigate the acquisition design that captures the time-lapse signal best, considering two types of setups, namely a surface-to-surface and a borehole-to-surface configuration.

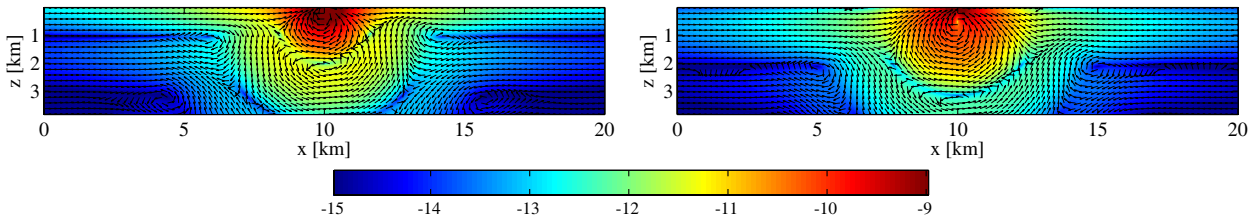

Figure 2: Current-density vector plots for a 2 Ohm·m half-space model. All panels show the x, z-plane at $y = 0$ km. A harmonic x-directed point dipole source (HED) is located at $(10, 0, 0)$ km. The source frequency is set to 1 Hz. The background color represents the amplitude of the current density on a logarithmic scale and the black arrows mark the directions of the current-density vectors. The left panel displays the real part of current density, whereas the right panel shows its imaginary part.

3. NUMERICAL EXPERIMENTS

Before considering a monitoring example, we start with a simple half-space configuration. Figure 2 shows vector plots of the current density for an x-directed point source (HED) in a vertical section of a homogeneous Earth model with a resistivity of 2 Ohm·m. The source is located at $(10, 0, 0)$ km, just below the air-earth interface, and operates at 1 Hz. The images illustrate the background current-density distribution. The color shows the magnitude of current density, overlayed by the black arrows that point in the direction of current-density vectors. The left panel shows the real part of current density, the right its imaginary part. In both panels, we see that the current-density distribution excited by a 1 Hz HED source rapidly decays away from the source. This clearly shows the diffusive character of EM fields generated by a low-frequency source. At shallow depth, both the real and imaginary parts of the current density are decaying less in the lateral direction. This fact is due to the so-called airwave, which is the electromagnetic field that propagates in the air with the speed of light. The part that propagates along the surface is called a lateral wave and it sends an electromagnetic field into the ground with an almost vertical diffusion direction [7]. A similar effect can be observed for a source at the interface between two conducting layers, where the fast diffusive medium (low conductivity) generates a field in the slow diffusive medium (high conductivity) that diffuses in the direction normal to the interface. The last case bears some resemblance to the refraction of seismic waves, where waves in the fast medium send energy back into the slow medium at the critical angle. A different pattern for the current-density distribution is obtained with a VED source, as shown in Figure 3. Here, we repeated the experiment but now with a z-directed point dipole source located at $(10, 0, 0.5)$ km. Unlike in the case of the HED source, the lateral wave is absent and the EM signals comprise only the direct field and the reflected fields due the air-earth interface, which acts as a perfect reflector [7]. If $\mathbf{E}^d$ denotes the direct EM field and $\mathbf{E}^{aw}$ the field related to the airwave, the HED source generates a field $\mathbf{E}^d + \mathbf{E}^{aw}$, whereas with a VED source only produces $\mathbf{E}^d$.

Next, we include a reservoir under production. We take the same half-space model as before and insert a 300-m thick resistive hydrocarbon-bearing layer at 1 km depth with a resistivity of 100 Ohm·m and a 200-m thick conductive water-bearing layer with a resistivity of 3 Ohm·m. The sketch of the reservoir is shown in Figure 4. For the monitoring study, we assume the reservoir is flooded by saline water from the top left, creating a small, 100-m thick, box-shaped depleted zone in the corner of the hydrocarbon-bearing layer.

The first experiment is with surface-to-surface configuration, placing a HED source on the surface and measuring the response with receivers also on the surface. The center panel of Figure 5 displays the amplitude behavior of time-lapse difference for the in-line electric field measured on the surface, excited by a HED point source located at $(11, 9.5, 0)$ km and operating at 1 Hz, as before. In this case, we assume the difference is entirely due the resistivity change in the reservoir.

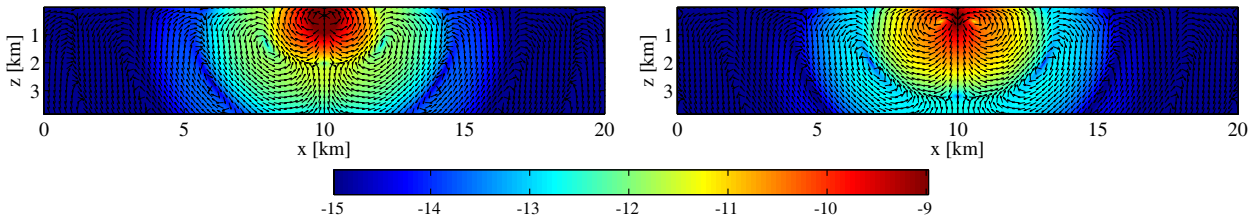

Figure 3: As Figure 2, but now for a z-directed point dipole source (VED), located at $(10, 0, 0.5)$ km.

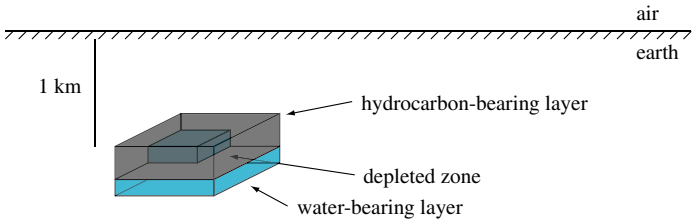

Figure 4: The reservoir has a dimension of 2 km by 2 km by 0.5 km, divided into two parts for oil-bearing reservoir and water-bearing reservoir. Before production, oil layer are assumed perfectly on top of water layer. During production, a part of oil layer is replaced by saline water creating a depleted zone in the top-left corner.

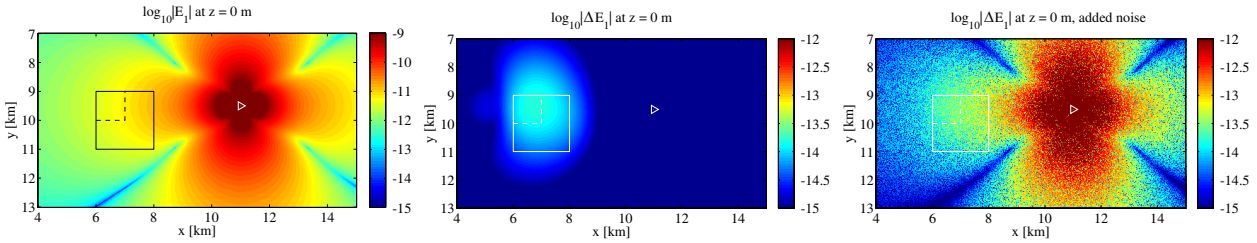

Figure 5: The left panel displays the x-directed electric field observed on the surface (top view), computed for the configuration that represents the resistivity before production. The center panel displays the time-lapse difference of the x-directed electric field observed on the surface (top view). The right panel displays the time-lapse difference with added noise. The solid white box indicates the lateral position of the reservoir and the dashed white line indicates the lateral position of the oil-water interface after flooding. The small white triangle marks the lateral location of the HED source.

Clearly, the result of the time-lapse difference is laterally confined to the location of resistivity change. However, if we compare the amplitude of time-lapse difference to its signal strength as shown in the left panel of Figure 5, we observe that the time-lapse signal is much weaker, below 1% of the signal strength. Consequently, the time-lapse difference may suffer from the multiplicative noise that would easily happen as a result of repeatability measurements. Frost, for instance, will increase the resistivity of the top soil and affect the time-lapse EM measurements. To illustrate the effect of this type of noise, we added a random number with a maximum amplitude of 1% relative to signal strength at each receiver, shown in the right panel of Figure 5. Here, we observed that the noise due the repeatability error dominates the time-lapse signal and imposes a strong source-imprint.

The multiplicative noise caused by repeatability errors can be described as follows. With time-lapse measurements, we collect two data sets, before and after production. The one obtained after production can be expressed as $\mathbf{E}^d + \mathbf{E}^{aw} + \mathbf{E}^{d;sc} + \mathbf{E}^{aw;sc}$. The first two terms denote the incident fields, consisting of a direct field and one due to the airwave. The last two scattering terms describe the time-lapse change. If we assume the time-lapse change is entirely due to the resistivity change in the reservoir, the component $\mathbf{E}^d + \mathbf{E}^{aw}$ will completely cancel out when considering the time-lapse difference. In the presence of multiplicative noise, however, the time-lapse difference will become $\alpha(\mathbf{E}^d + \mathbf{E}^{aw}) + \mathbf{E}^{d;sc} + \mathbf{E}^{aw;sc}$, where the factor α models the repeatability errors. The noise becomes a problem if $|\mathbf{E}^{d;sc} + \mathbf{E}^{aw;sc}|$ is much smaller than $|\alpha(\mathbf{E}^d + \mathbf{E}^{aw})|$, as happens in Figure 5. In that case, the airwave, $\mathbf{E}^{aw}$, appears as the predominant signal.

Let us assume that the time-lapse difference is entirely due the resistivity changes in the reservoir, so that it can be written as $\mathbf{E}^{d;sc} + \mathbf{E}^{aw;sc}$. We want to determine which of the two incident fields, $\mathbf{E}^d$ or $\mathbf{E}^{aw}$, most affects the time-lapse signal. To reduce the contribution of the direct field, we placed the source further away from the target, whereas to reduce the contribution of the airwave, we repeated the experiment in a fully homogeneous background, without an air-earth interface. Figure 6 shows the results. The leftmost panel displays the time-lapse difference when we have the contributions of both the direct field and the airwave. The center panel shows the time-lapse difference when we have only the airwave contribution and the rightmost with only the direct field. Clearly, the time-lapse signal due to the incident field generated by the airwave provides the best result. We also observe that the time-lapse difference measured on the surface is laterally confined to the location of resistivity changes in that case. Therefore, the presence of the airwave is beneficial, because it illuminates the depleted zone even if the source is not close to the target. In the presence of repeatability errors, however, the strong currents induced by the incident airwave cannot be fully subtracted and the multiplicative noise will start to dominate the time-lapse signals, making them difficult to detect.

As an alternative, we considered a vertical dipole source located in a well. The left panel of Figure 7 displays the amplitude behavior of time-lapse differences for the in-line electric field measured on the surface, excited by a VED point source located at $(11, 9.5, 0.5)$ km and operating at 1 Hz, as before. The right panel of Figure 7 displays the same response, but after adding random noise with a maximum amplitude of 1% relative to the signal strength at each receiver. The time-lapse differences can still be recognized, although not easily.

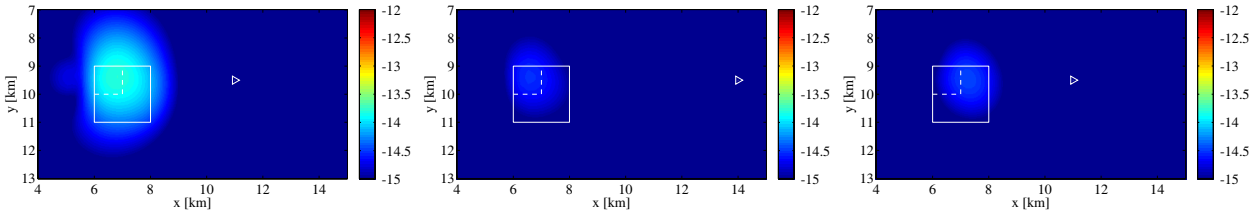

Figure 6: All panels show $\log_{10}|\Delta E_1|$ at $z = 0\,\text{km}$ (top view). The leftmost panel displays the amplitude behavior of time-lapse difference when the resistivity change is illuminated by the direct field and the airwave. The center panel corresponds to illumination by only the airwave, and the rightmost panel by only the direct field.

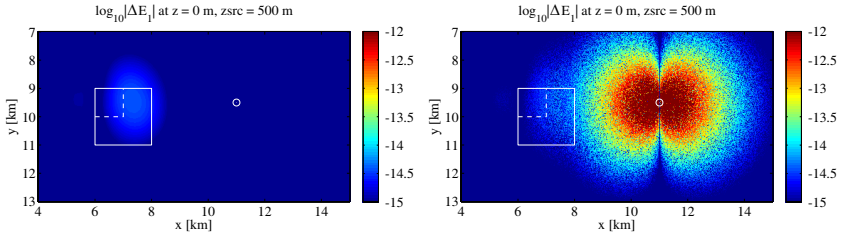

Figure 7: The left panel displays the time-lapse differences of the electric component E_1 observed on the surface (top view). The right panel displays the time-lapse difference of the electric component E_1 with added noise.

4. CONCLUSIONS

With the HED source, the airwave appears as the predominant signal. It propagates in the air and the part that propagates parallel to the surface has a geometrical spreading function inversely proportional to distance squared. This part generates a diffusive electromagnetic field that diffuses almost vertically down into the Earth. The presence of the airwave can be beneficial for the monitoring problem, because it provides illumination of the depleted zone even if the source is not close to the target. However, at the same time, the strong currents induced by the airwave also dominate the time-lapse signals. In the presence of repeatability errors, this will make it difficult to recognize the signals due to time lapse changes in the presence of repeatability errors. However, a HED source could still be useful if the airwave can be eliminated or at least be reduced. Otherwise, placing the source in a vertical well is the preferred option, in spite of the higher cost.

ACKNOWLEDGMENT

Marwan Wirianto received financial support from the sponsors of the Delphi consortium.

REFERENCES

1. Constable, S. and L. J. Srnka, "An introduction to marine controlled-source electromagnetic methods for hydrocarbon exploration," *Geophysics*, Vol. 72, No. 2, WA3–WA12, 2007.
2. Black, N. and M. S. Zhdanov, "Monitoring of hydrocarbon reservoirs using marine CSEM method," *SEG Technical Program Expanded Abstracts: 79th Annual International Meeting*, 850–854, Houston, USA, October 2009.
3. Lien, M. and T. Mannseth, "Sensitivity study of marine CSEM data for reservoir production monitoring," *Geophysics*, Vol. 73, No. 4, F151–F163, 2008.
4. Orange, A., K. Key, and S. Constable, "The feasibility of reservoir monitoring using time-lapse marine CSEM," *Geophysics*, Vol. 74, No. 2, F21–F29, 2009.
5. Wirianto, M., W. A. Mulder, and E. C. Slob, "A study of land CSEM reservoir monitoring in a complex 3D model," *71st EAGE Conference & Exhibition Incorporating SPE EUROPEC 2009, Extended Abstract*, X020, Amsterdam, 2009.
6. Mulder, W. A., "A multigrid solver for 3D electromagnetic diffusion," *Geophysical Prospecting*, Vol. 54, No. 5, 633–649, 2006.
7. King, R. W., M. Owens, and T. Wu, *Lateral Electromagnetic Waves: Theory and Applications to Communications, Geophysical Exploration, and Remote Sensing*, Springer-Verlag, Inc., New York, 1992.